HYDROLOGICAL PROCESSES
Hydrol. Process. **27**, 1572–1589 (2013)
Published online 11 May 2012 in Wiley Online Library
(wileyonlinelibrary.com) DOI: 10.1002/hyp.9220

Assessment of hydrologic impacts of climate change in Tunga–Bhadra river basin, India with HEC-HMS and SDSM

R. Meenu,[1] S. Rehana[1] and P. P. Mujumdar[1,2]*

[1] *Department of Civil Engineering, Indian Institute of Science, Bangalore 560 012, India*
[2] *Divecha Center for Climate Change, Indian Institute of Science, Bangalore 560 012, India*

Abstract:

Climate change would significantly affect many hydrologic systems, which in turn would affect the water availability, runoff, and the flow in rivers. This study evaluates the impacts of possible future climate change scenarios on the hydrology of the catchment area of the Tunga–Bhadra River, upstream of the Tungabhadra dam. The Hydrologic Engineering Center's Hydrologic Modeling System version 3.4 (HEC-HMS 3.4) is used for the hydrological modelling of the study area. Linear-regression-based Statistical DownScaling Model version 4.2 (SDSM 4.2) is used to downscale the daily maximum and minimum temperature, and daily precipitation in the four sub-basins of the study area. The large-scale climate variables for the A2 and B2 scenarios obtained from the Hadley Centre Coupled Model version 3 are used. After model calibration and testing of the downscaling procedure, the hydrological model is run for the three future periods: 2011–2040, 2041–2070, and 2071–2099. The impacts of climate change on the basin hydrology are assessed by comparing the present and future streamflow and the evapotranspiration estimates. Results of the water balance study suggest increasing precipitation and runoff and decreasing actual evapotranspiration losses over the sub-basins in the study area. Copyright © 2012 John Wiley & Sons, Ltd.

KEY WORDS climate change impacts; hydrologic model; statistical downscaling; HEC-HMS; SDSM

Revised 4 December 2011; Accepted 15 December 2011

INTRODUCTION

The increasing awareness that enhanced levels of greenhouse gases of direct/natural or indirect anthropogenic origin in earth's atmosphere might change the climate of different regions of the world, in the long run, has recently instigated a great deal of research into the projection of regional responses to global climate change. Various general circulation model (GCM) experiments and studies indicate that a substantial rise in global temperature would be expected as a consequence of a doubling of carbon dioxide (CO_2) concentrations. As a result, climatic processes are likely to intensify, including the severity of hydrological events such as droughts, flood waves, and heat waves. These projected effects of possible future climate change would significantly affect many hydrologic systems, which in turn affect the water availability and runoff and the flow in rivers. Hence, an assessment of the possible impacts of climate change on the hydrology of a basin is essential in the wake of global warming.

Physically based distributed hydrological models designed to understand and approximate the general internal processes and physical mechanisms, which govern the hydrologic cycle and incorporate the physical laws of water movement and the parameters associated with the characteristics of the catchment area (Sorooshian and Gupta, 1995), have been found to be useful for such impact assessment studies. By simulating streamflow from precipitation and temperature data derived from GCM outputs corresponding to the specific climate change scenarios, using a suitable hydrological model, it is possible for one to quantify the corresponding changes in the hydrology of the basin. However, the projections of the estimates of these climate variables for a future period obtained directly from GCMs are of limited value for any study as the spatial resolution of GCM is too coarse to resolve many sub-grid scale hydrological processes and because the output is always unreliable at individual grid. Spatial downscaling methods have been proposed to solve this problem. The methods used to convert GCM outputs into local meteorological variables used for hydrological modelling are referred to as downscaling techniques (Dibike and Coulibaly, 2005; Xu *et al.*, 2009). The widely used method of statistical downscaling involves bridging of the two different scales by establishing empirical relation between large-scale variables reliably simulated by the GCMs at grid-box scales (e.g. mean sea level pressure and geopotential height fields) and local climate variables (e.g. temperature and precipitation at a location). Statistical downscaling has a number of advantages over the use of raw GCM output because of the stochasticity of the downscaling model, ability to reproduce the unique meteorological characteristics of the individual stations, and finally being less data intensive than dynamical methods such as nested or regional climate modelling (Wilby *et al.*, 1999).

*Correspondence to: P. P. Mujumdar, Department of Civil Engineering, Indian Institute of Science, Bangalore 560 012, India.
E-mail: pradeep@civil.iisc.ernet.in

In the recent years, a great deal of research has gone into the field of assessment of impacts of climate change on hydrological processes. Yimer *et al.* (2009) provided downscaled meteorological variables corresponding to global emissions scenario (A2a) as input to the calibrated and validated Hydrologic Engineering Center's Hydrologic Modeling System (HEC-HMS) hydrological model to simulate the corresponding future streamflow changes in the Beles River in Ethiopia. The physically based model HEC-HMS had been pointed out as being a standard model in the private sector in the USA for the design of drainage systems, quantifying the effect of land use change in flooding, etc. (Singh and Woolhiser, 2002). It is known to be a very adaptable software as it includes a variety of model choices for each segment of the hydrologic cycle. Jiang *et al.* (2007) in his study investigated the potential impacts of anthropogenic climate change on the water availability in the Dongjiang basin, South China. Six monthly water balance models, namely the Thornthwaite–Mather (TM), Vrije Universitet Brussel (VUB), Xinanjiang (XAJ), Guo (GM), WatBal (WM), and Schaake (SM) models are used, and their capabilities in reproducing historical water balance components and in predicting hydrological impacts of alternative climates are compared. Jha *et al.* (2006) used the Soil Water Assessment Tool (SWAT) to assess the impact of simple sensitivity scenarios and a suite of climate change scenarios on the hydrologic response of Upper Mississippi River Basin. Christensen *et al.* (2004) studied the potential effects of climate change on the hydrology and water resources of the Colorado River basin by comparing simulated hydrologic and water resources scenarios derived from downscaled transient temperature and precipitation sequences extracted from PCM simulations. The variable infiltration capacity (VIC) macroscale hydrology model was used to produce corresponding streamflow sequences. Yu and Wang (2009) investigated the impact of climate change on rainfall, evapotranspiration, and discharge in northern Taiwan. The daily rainfall and temperature series obtained from delta change of monthly temperature and precipitation from the grid cell of GCMs were input into the calibrated HBV-based hydrological model to project the hydrological variables.

The Statistical DownScaling Model (SDSM), a regression-based downscaling model, involves developing quantitative relationships between large-scale atmospheric variables (predictors) and local surface variables (predictands). Chu *et al.* (2010), in his study, applied SDSM to the Haihe River basin, China, and investigated its applicability by downscaling mean temperature, pan evaporation, and precipitation, which are important for assessing the impact of climate change on water resource management. Dibike and Coulibaly (2007) investigated the potential of two hydrological models WatFlood and HBV-96 for climate change impact studies by validating them with meteorological inputs from both the historical records and the SDSM downscaled outputs.

River Tunga–Bhadra is a tributary of Krishna river in India. Very few studies on the hydrological modelling of Tunga–Bhadra river basin have been reported so far. The study conducted in the Tunga–Bhadra basin by Rehana and Mujumdar (2011) on the impacts of climate change on water quality variables by using hypothetical climate change scenarios reported a decreasing trend in the streamflows in the historical period itself. All the hypothetical climate change scenarios projected a deterioration of water quality. It was found that there is a significant decrease in dissolved oxygen levels due to the impact of climate change on temperature and flows.

The present study aims at assessing the impacts of potential future climatic changes on the hydrology of the catchment area of Tunga–Bhadra River, lying upstream of the Tungabhadra dam. Firstly, a hydrological model of the study area is developed using the HEC-HMS version 3.4, a physically based, semi-distributed model. Then, downscaling of the meteorological variables obtained as output from the Hadley Centre Coupled Model version 3 (HadCM3) GCM for Special Report on Emissions Scenarios (SRES) A2 and B2 scenarios is performed using SDSM 4.2, a regression-based downscaling tool. The hydrological model is validated for the baseline period with the downscaled output of GCMs. The assessment of impacts of climate change on the study area is carried out by incorporating the future rainfall and temperature data downscaled using SDSM 4.2 into the HEC-HMS 3.4 model. The changes in simulated streamflows, evapotranspiration, and water balance in the study area between current and future scenarios are investigated.

STUDY AREA AND DATA SETS

Study area

The Tunga–Bhadra River is formed north of Shimoga, in the state of Karnataka, India at an elevation of about 610 metres by the union of twin rivers, the Tunga and the Bhadra. The major tributaries of the river are Bhadra, Tunga, and Varada. The catchment area taken up in this study lies in the upstream of the Tungabhadra dam and spans over about 15 600 km^2. A map of Tunga–Bhadra basin is shown in Figure 1. The upper catchments are characterized by undulating terrain and much higher rainfall; the middle portion of the basin has much lower rainfall, drought conditions, not so undulating terrain, and mainly plains. The average slope of the basin is 6%. The basin is dominated by clay loam soil with the soil composition in the area: 42% clay loam, 34% clayey soil, and 19% sandy clay soil. Farm land is the main land use/land cover in the Tunga–Bhadra basin in Karnataka state as of 2004–2005, accounting for more than 55% of the surface. Other cultivable areas such as trees and groves, fallow land, and cultivable waste add up to 12.5% of the territory. Forests and natural vegetation cover 16% of the area, and around 5% is used as permanent pastures. Eleven percent of the territory is not available for cultivation or for natural vegetation (Source: STRIVER Task Summary Report No. 9.3, http://kvina.niva.no/striver/Disseminationofresults/STRIVERReports/tabid/80/

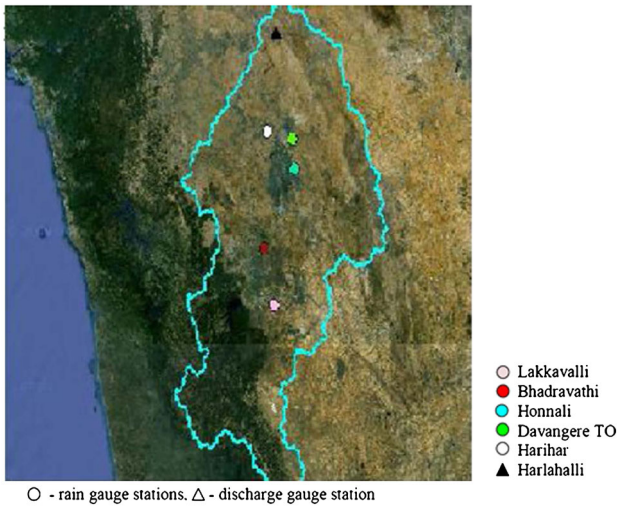

Figure 1. Map of Tunga–Bhadra Basin and gauge locations (source: Google Earth (2010,2009))

Default.aspx). As most part of the Tunga–Bhadra catchment is located in the centre of the Peninsula, the basin receives an average of 1024 mm of rainfall in a year. The annual average temperature reaches 26.7 °C. In general, humidity is high during the monsoon period and comparatively low during the post monsoon period. In summer, the weather is dry and the humidity is low. The relative humidity in the basin ranges from 17% to 92%.

Data used

The characteristics of the river basin, i.e. land use, properties of soil, etc., are held constant throughout the simulation period, and estimates of various soil parameters are obtained from available literature on the study area. The study area is divided into four sub-basins on the basis of the soil cover and land use. The soil cover data obtained from HWSD Viewer 1.1 (2009) and the land use–land cover data available from the case study by STRIVER (2009) is combined to obtain estimates of various soil layer and hydrological properties of the soil such as saturated hydraulic conductivity, maximum moisture deficit, percentage of impervious space, basin lag, crop coefficient, and dryness coefficient. The exact estimate of each of these values for each sub-basin is obtained during calibration. The various properties of these sub-basins are given in Table I.

Climatic data required in the study are daily precipitation, maximum and minimum air temperature, and solar radiation. Maximum and minimum temperatures are obtained from the India Meteorological Department (IMD). Precipitation records of five rain gauge stations (Bhadravathi, Lakkavalli, Davanagere TO, Honnali TO, and Harihar located in the Tunga–Bhadra basin) are obtained from the IMD. Historical precipitation and temperature data are available for the period 1960–2003 and 1969–2003, respectively. The radiation data required by the hydrological model are not available directly, so net radiation is calculated using empirical equation. The relationships for calculation of daily net radiation from solar radiation and weather data by the United Nations Food and Agriculture Organization's recommended method are used in the study. The required inputs are the Julian date, latitude, and maximum and minimum temperatures. The streamflow data for the period 1972–2003 recorded at the Harlahalli gauging site located near the outlet of the watershed is used as the observed flows and is obtained from the Karnataka State Water Resources Development Organization.

Table I. Values of important parameters present in the hydrological model

Sub-basin	Area (km^2)	Type of soil	Constant loss rate (mm/h)	Impervious percent	Crop coefficient
1	3259	Nitisols (loam + sandy clay loam)	0.6–3.4	13.77	1.15
2	883.3	Vertisols (light clay + loam)	0.001–1.3	10.77	0.95
3	5662	Luvisols (loam + light clay)	1.3–3.8	15.77	1.1
4	5860	Plinthosols (loam)	1.3–3.8	10.77	1.0

The observed large-scale atmospheric predictors for the baseline period are derived from the National Centre for Environmental Protection (NCEP) reanalysis data set. The baseline period selected is 1961–1990, the standard World Meteorological Organization period, as it incorporates the natural variability of the climate (Xu *et al.*, 2009). The GCM used in this study is the HadCM3, which is a coupled atmosphere–ocean GCM developed at the Hadley Centre in the UK. The outputs of HadCM3 A2 and B2 emissions scenarios described in the SRES prepared by the Intergovernmental Panel on Climate Change (IPCC) are used in this study. The NCEP/NCAR reanalyses have a grid-spacing of 2.5° latitude by 2.5° longitude whereas the HadCM3 has a resolution of 2.5° latitude by 3.75° longitude. So, the NCEP reanalysis predictors have to be re-gridded to conform to the grid-spacing of HadCM3, using the weighted average of neighbouring grid-points. The standardization of predictors is widely used prior to statistical downscaling to reduce biases in the mean and variance of GCM atmospheric fields relative to observations or reanalysis data. The re-gridded and standardized predictors used as the SDSM model input are obtained from the Canadian Climate Impacts Scenarios Group website (http://www.cics.uvic.ca/scenarios/sdsm/select.cgi). The predictor variables are supplied on a grid basis, and the data for the particular grid are extracted for three distinct periods, namely, the 2020s (2011–2040), the 2050s (2041–2070), and the 2080s (2071–2099).

HYDROLOGICAL MODELLING USING HEC-HMS 3.4

Model setup

The model used in this study, HEC-HMS 3.4, developed by United States Army Corps of Engineers, is designed to simulate the precipitation–runoff processes of dendritic watershed systems. HEC-HMS model setup consists of a

basin model, meteorologic model, control specifications, and input data (time series data). The study area is divided into four sub-basins, and they are characterized by different soil type and land use pattern. The physical watershed is represented in the basin model as in Figure 2.

For this particular study, *deficit and constant loss* model is used to compute the losses from the watershed. The deficit and constant loss model uses a single soil layer to account for continuous changes in moisture content. It is a quasi-continuous model and has to be used in conjunction with a meteorological model that computes evapotranspiration (US Army Corps of Engineers, 2008). The parameters for this model include initial deficit, maximum deficit, constant rate, and impervious percentage. In order to compute direct runoff from excess precipitation, one should use a transform method. In this study, *SCS unit hydrograph* model is used to transform the flows. Soil Conservation Service Unit Hydrograph (SCS UH) model is a parametric UH model, based upon the averages of UH derived from gauged rainfall and runoff for a large number of small agricultural watersheds throughout the SCS. The input parameter for this method is the basin lag, which is 0.6 times the time of concentration of the flow. The *constant monthly baseflow* method is used to account for the baseflows. It represents base flow as a constant flow; this may vary monthly.

In the present study, the spatio-temporal precipitation distribution is accomplished by the gauge weight method. This method uses separate parameter data for each gauge used to compute precipitation and also uses separate parameter data for each sub-basin in the meteorologic model. The meteorologic model uses Priestley–Taylor evapotranspiration method as input for continuous hydrological simulation. The data requirements are limited to the maximum and minimum temperature, solar radiation, crop coefficients, and dryness coefficient. The model assumes that no evapotranspiration losses take place in the basin during periods of precipitation. The control specifications model specifies the start and end of the computation period and the computation time interval. The computation time interval is daily. Time windows are created for the calibration and validation periods.

Model calibration and validation

Split sample procedure is followed in the model testing. Twenty years (1973–1992) of observed streamflow data are used for calibrating the hydrological model and remaining 10 years data (1993–2002) for validation. The characteristics of the river basin, i.e. land use, properties of soil, etc., are held constant throughout the simulation period. The constant loss rate and maximum deficit parameters, needed for the deficit and constant loss method, and the basin lag parameter in SCS unit hydrograph transform method are taken into consideration in the simulation. The peak weighted root mean square function is chosen as the objective function, and the Nelder and Mead algorithm is used to minimize the objective function.

Performance evaluation of the model

The statistics of the flows such as mean, standard deviation, normalized root mean squared error NRMSE, and covariance of root mean squared error CVRMSE are compared. The model performance efficiency criteria such as coefficient of determination R^2, Nash–Sutcliffe model efficiency E (Nash and Sutcliffe, 1970), and percent deviation D are used to evaluate the model simulations during the calibration and validation periods. The R^2 value indicates the correlation between the observed and simulated values, and E measures how well the plot of the observed against the simulated flows fits the 1 : 1 line. The R^2 coefficient is calculated using Equation 1.

$$R^2 = \frac{\sum\left(Q_{\text{obs}} - \overline{Q_{\text{obs}}}\right) \times \left(Q_{\text{sim}} - \overline{Q_{\text{sim}}}\right)}{\sqrt{\left(\sum\left(Q_{\text{obs}} - \overline{Q_{\text{obs}}}\right)^2 \times \left(Q_{\text{sim}} - \overline{Q_{\text{sim}}}\right)^2\right)}} \quad (1)$$

where Q_{sim} is the simulated value, Q_{obs} is the observed value, $\overline{Q_{sim}}$ is the average simulated value, and $\overline{Q_{obs}}$ is the average observed value. The range of values for R^2 is 1.0 (best) to 0.0 (unacceptable).

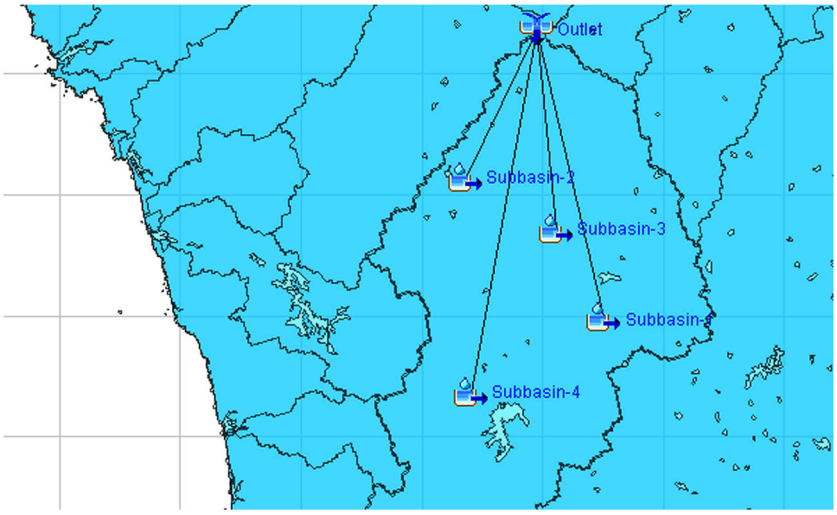

Figure 2. Basin model in the HEC-HMS 3.4 hydrological model showing the four sub-basins and the outlet in the study area

The E value is calculated using Equation 2. If the E value is less than or close to zero, the model simulation is unacceptable. The best value is 1.

$$E = 1 - \frac{\sum(Q_{obs} - Q_{sim})^2}{\sum\left(Q_{obs} - \overline{Q_{obs}}\right)^2} \quad (2)$$

The percent deviation of streamflows (D) over a specified period with total days calculated from measured and simulated values of the quantity in each model time step is determined using Equation 3.

$$D = 100 \times \frac{Q_{obs} - Q_{sim}}{Q_{obs}} \quad (3)$$

A value close to 0% is best for D. A negative value indicates model overestimation, and a positive value indicates model underestimation.

STATISTICAL DOWNSCALING USING SDSM 4.2

Statistical downscaling methods establish empirical relationships between GCM-resolution climate variables and local climate in a simplified form as in Equation 4:

$$R = F(L) \quad (4)$$

where R is the predictand (a local climate variable), L is the predictor (a set of large-scale climate variables), and F a deterministic/stochastic function conditioned by L and is estimated empirically from historical observations.

The present study used SDSM 4.2 to downscale the maximum and minimum temperature and daily mean areal precipitation in the four sub-basins of the study area. *Quality Control* check in SDSM is performed on the maximum and minimum temperature data and mean areal precipitation data of all the sub-basins in the basin to identify errors in the data records, specifically missing data if any, using codes, and outliers prior to model calibration. The predictor variable, mean temperature lagged by 1 day (t_lag), is created using *Transform* feature. As the distribution of precipitation is skewed, a fourth root transformation is applied to the original series to convert it to the normal distribution and then used in the regression analysis. The screening of predictors is performed using the results of seasonal correlation analysis, partial correlation analysis, and scatter plots. The model structure is specified as monthly and the downscaling process as unconditional or conditional. Minimum and maximum temperatures are modelled as unconditional processes. Precipitation is modelled as a conditional process in which the local precipitation amount is correlated with the occurrence of wet days. Auto-regression option is also selected in order to include an auto-regressive term in the regression equations for downscaling temperatures. The correlation analysis is used to investigate inter-variable correlations for specified sub-periods (annual, seasonal, or monthly). On the basis of the correlation values and scatter plots, the predictors selected suitable for downscaling the temperatures and daily precipitation values for this case study are listed in the Table II.

The *Calibrate Model* takes up each of the predictand and a set of probable predictors and computes the parameters of multiple regression equations by using an optimization algorithm (ordinary least squares). Monthly model type is selected in which different model parameters are derived for each month. From the 30 years of data representing current climate (1961–1990), the 11 years of data (1969–1979) are used for calibrating the regression model whereas 10 years of data (1981–1990) are used to validate the model. The summary screen reports the percentage of explained variance, the standard error (SE) for the model, and Durbin–Watson statistic for each month. Once the explained variance and SE values obtained are found satisfactory, the regression model is finalized.

About five ensemble members of each variable for the validation period are synthesized using the *Weather generator*. Thus, verification of the calibrated models (using independent data) is carried out. SDSM 4.2 facilitates comparison of downscaled scenarios and observed climate data with the *Summary Statistics* and *Frequency Analysis* screens. Statistical analysis of both observed and synthetic data are performed using the variable mean, maximum, minimum, variance, percent wet-days, and dry-day spell lengths, etc. computed on monthly, seasonal, or annual basis. The *Compare Results* screen enables us to plot monthly statistics produced by the *Summary Statistics* screen. During the calibration and the validation of downscaling models for precipitation, the mean daily precipitation and daily precipitation variability for each month, monthly average percent of wet days, and dry-spell lengths are used to evaluate the performance of model. For the evaluation of the performance of the regression models for temperature, mean values of observed and NCEP simulated data are compared.

The *Scenario Generator* operation produces ensembles of downscaled synthetic daily weather series given atmospheric predictor variables supplied by the GCM HadCM3 (either for present or future climate experiments). About five ensemble members of each climate variable are downscaled for the A2 and B2 scenarios of HadCM3 model by using the corresponding set of predictor variables. As HadCM3 has year lengths of 360 days, the downscaled variables will have each year of 360 days. The output from SDSM has to be processed outside the model to convert it into 365 days in a year form, so that it is ready to be input into the hydrological model. The statistical downscaling results obtained for the future are analysed and projections for future are made. The maximum and minimum monthly temperature and mean areal daily rainfall for the baseline and future time slices (2020s, 2050s, and 2080s) are computed and compared. The projections are made for monthly rainfall, percentage of wet days, and dry-spell length also.

Table II. Predictands and their selected NCEP predictors

T1 (sub-basin 1)		T2 (sub-basins 2 and 3)		T3 (sub-basin 4)		R1 (sub 1)	R2 (sub 2)	R3 (sub 3)	R4 (sub 4)
Max	Min	Max	Min	Max	Min				
mslp	p_z	mslp	mslp	p500	p_u	p_f	mslp	mslp	mslp
p_f	p5_v	p5_f	p5zh	p850	p500	p_zh	p_f	p_zh	p_f
p_u	p500	p8_v	p8_f	tlag	r500	p8_f	p_zh	p8_f	p_zh
p_zh	p8zh	p850	p8_u		rhum	r500	p8_f	p8th	p8_u
p500	rhum	shum	p8_z		shum	r850	r850	r500	p850
p8_f	shum	tlag	p8zh		tlag	rhum	rhum	r850	r500
p850	tlag		rhum			shum	shum	rhum	r850
p8zh			shum					shum	rhum
tlag			tlag						

Note:

- Predictands used in the study:
  1. Maximum and minimum temperatures in the four sub-basins of the study area, i.e. T1-max and T1-min (in sub-basin 1), T2-max and T2-min (in sub-basins 2 and 3), T3-max and T3-min (in sub-basin 4).
  2. Mean areal precipitation at daily time step in the four sub-basins of the study area: precipitation R1, R2, R3, and R4 in sub-basin 1, sub-basin 2, sub-basin 3, and sub-basin 4, respectively.
- NCEP predictors provided by SDSM:
  1. mean sea level pressure (mslp)
  2. 2 m near surface temperature (temp)
  3. 2 m near surface temperature lagged 1 day (t_lag)
  4. 500 hPa geopotential heights (p500)
  5. 850 hPa geopotential heights (p850)
  6. near surface-specific humidity (shum)
  7. specific humidity
     (i) at 500 hPa height (s500)
     (ii) at 850 hPa height (s850)
  8. near surface relative humidity (rhum)
  9. relative humidity
     (i) at 500 hPa height (r500)
     (ii) at 850 hPa height (r850)
  10. geostrophic air flow velocity
     (i) at the surface (p_f)
     (ii) at 850 hPa height (p8_f)
     (iii) at 500 hPa height (p5_f)
  11. vorticity
     (i) at the surface (p_z)
     (ii) at 850 hPa height (p8_z)
     (iii) at 500 hPa height (p5_z)
  12. zonal velocity component
     (i) at the surface (p_u)
     (ii) at 850 hPa height (p8_u)
     (iii) at 500 hPa height (p5_u)
  13. meridional velocity component
     (i) at the surface (p_v)
     (ii) at 850 hPa height (p8_v)
     (iii) at 500 hPa height (p5_v)
  14. divergence
     (i) at the surface (p_zh)
     (ii) at 850 hPa height (p8_zh)
     (iii) at 500 hPa height (p5_zh)

ASSESSMENT OF IMPACTS OF CLIMATE CHANGE USING THE HYDROLOGICAL MODEL

The comparison of water balance, evapotranspiration, and streamflow of present and future conditions is performed in order to quantify the changes in hydrology of the watershed due to future climate change. This is achieved by simulating the future hydrology of the basin by using the hydrological model.

Even though the hydrological model used in the study is found capable of reproducing the historical streamflow record reasonably well, its application to predict the hydrology of streams in future climate depends on its ability to model the current scenarios (Dibike and Coulibaly, 2007). The downscaled baseline temperature and precipitation obtained from SDSM is input into the model to simulate the baseline streamflows. The average monthly observed streamflows, simulated streamflows using observed inputs, and baseline streamflows for the period 1973–1990 are compared to validate the model. The validated hydrological model is used to generate the streamflows at the outlet and potential evapotranspiration (PET) in the four sub-basins of the study area for the current as well as future periods by using the downscaled temperature and precipitation data corresponding to the A2 and B2 scenarios developed by the HadCM3. No change in soil cover or land use pattern is assumed for the future scenarios. This makes it sure that the projections

for future are entirely dependent on the climate change scenarios. The impacts of climate change on the streamflows, PET, and water balance of the study area are then investigated.

RESULTS AND DISCUSSIONS

Hydrological modelling

Calibration and validation of HEC-HMS. The calibration of HEC-HMS 3.4 model for the study area is carried out by comparing the simulated daily streamflows with the observed flow at the outlet of the basin. As a large number of parameters are involved, on the basis of a sensitivity analysis, three parameters, namely the hydraulic conductivity of the soil (mm/h), maximum moisture deficit (mm), and time lag (min), in each sub-basin are identified for calibrating the model. The statistics of the observed and HEC-HMS 3.4 simulated daily flows during calibration and validation periods are shown in Table III. The mean values of daily flows are simulated very well by the model during both periods. Peak flow is underestimated during the validation period.

The plots of observed and simulated daily flows as well as monthly flows are given in Figures 3 and 4. It shows daily flows are well simulated in some of the calibration years, as in 1973, 1977, and 1988, but most of the high flows in the JJAS (June–July–August–September) period are underpredicted by the model. Underprediction of high flows is present in almost all the validation years too. This discrepancy has already been observed by previous studies of hydrological modelling (for example, Yimer, *et al*., 2009). The results of an investigation into the extent and magnitude of underprediction of high flows (that is, the flows in the months of June to September or JJAS period) is given in Table IV. The results indicate that during calibration and validation periods, 33.5% and 30.4% of the high flows, respectively, are underestimated, that is, the simulated high flows are below 85% of the magnitude of the observed high flows. This addresses the uncertainty involved in the simulations of the model. The various performance evaluation measures computed for the daily and monthly streamflows in the calibration and validation periods are listed in the Table V. The R^2 and E values for the calibration period are 0.72 and 0.48, respectively, but slightly improved during the validation period for daily flows. Value of D of less than 2% indicates a negligible underestimation of total flows.

Table III. Statistics of the observed and simulated daily flows

Statistic (cumecs)	Streamflows (cumecs)			
	Calibration period (1973–92)		Validation period (1993–02)	
	Observed	Simulated	Observed	Simulated
Maximum	7358.0	7402.0	5842.0	3238.0
Mean	233.1	233.0	225.8	221.3
SD	412.8	370.7	416.0	327.2

SD, standard deviation.

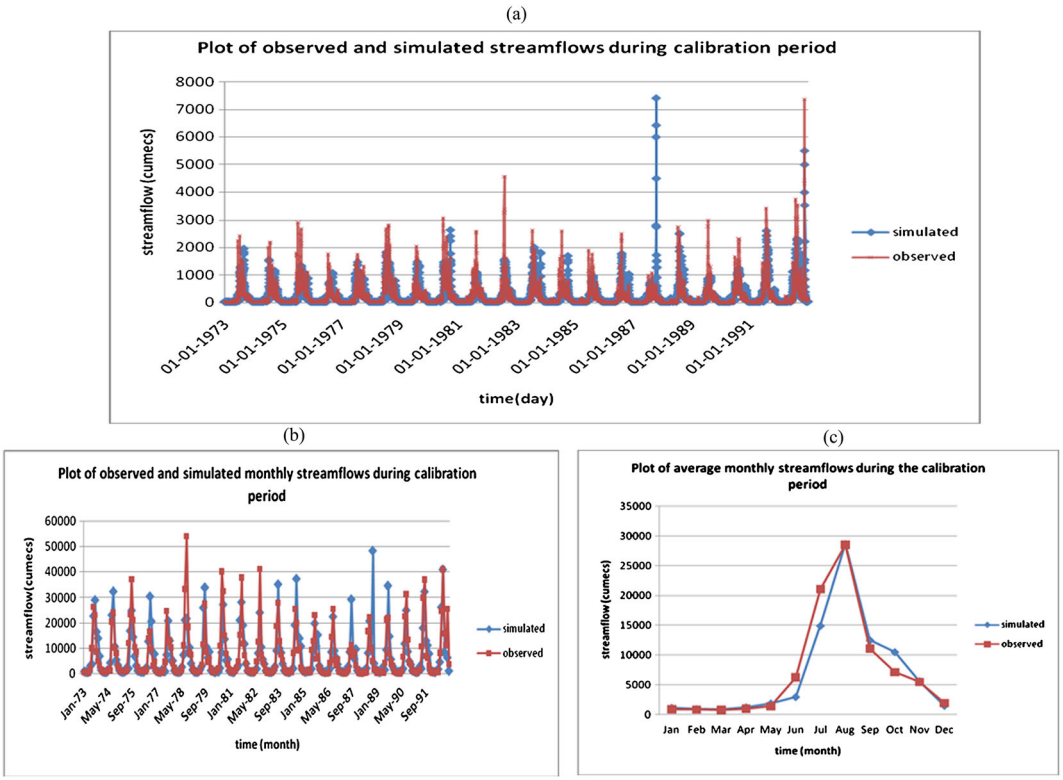

Figure 3. Comparison plots of observed and simulated (a) daily, (b) monthly, and (c) average monthly streamflows at the outlet of the basin during the calibration period (1973–1992)

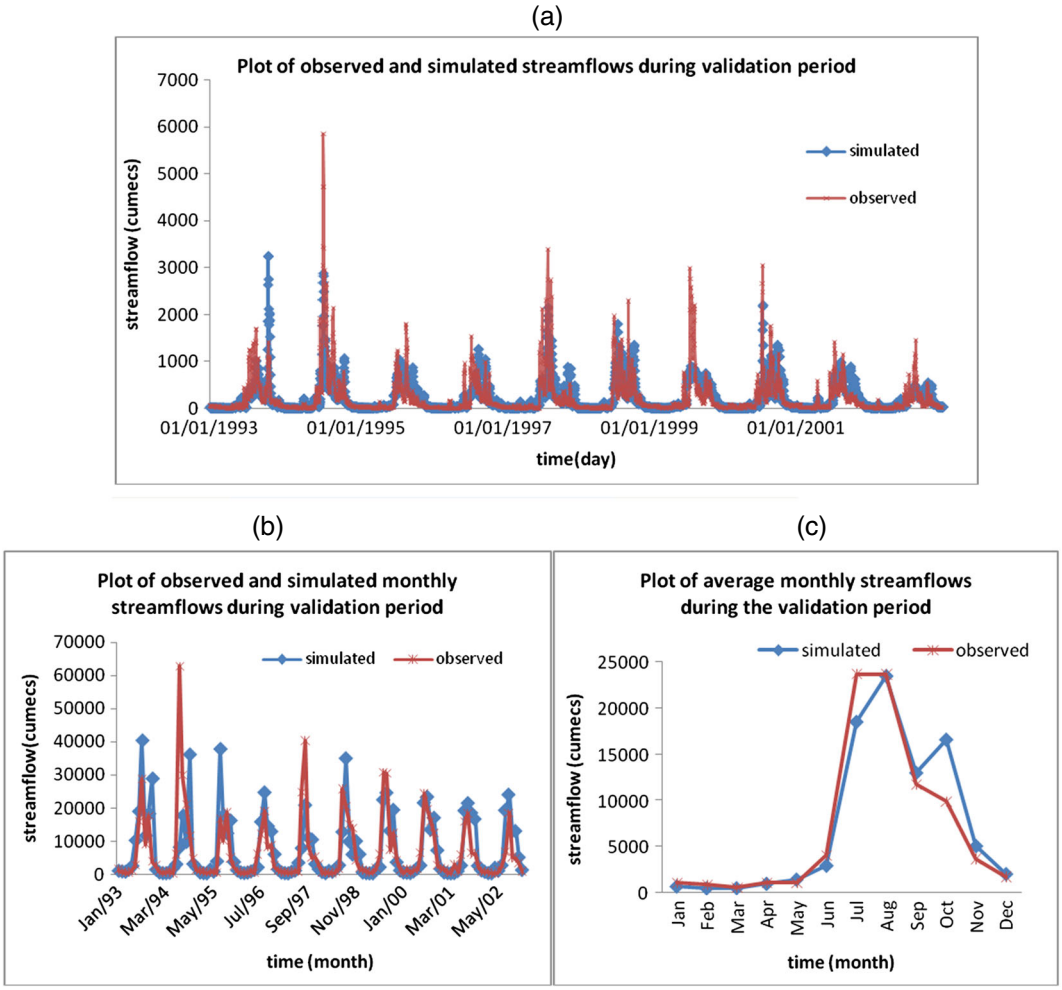

Figure 4. Comparison plots of observed and simulated (a) daily, (b) monthly, and (c) average monthly streamflows at the outlet of the basin during the validation period (1993–2002)

Table IV. Percentage and magnitude of underprediction in high flows

Magnitude of observed flow (%)		75	80	85	90	95
Percent of underpredicted flows	Calibration	26.2	29.9	33.5	37.4	40.4
	Validation	24.6	27.4	30.4	33.3	35.8

Table V. Performance assessment of HEC-HMS 3.4 model during calibration and validation

Test statistic	Daily streamflows		Monthly streamflows	
	Calibration period (1973–1992)	Validation period (1993–2002)	Calibration period (1973–1992)	Validation period (1993–2002)
R^2	0.72	0.77	0.87	0.88
E	0.48	0.59	0.75	0.78
D (%)	0.07	1.96	0.07	1.96
NRMSE	0.04	0.05	0.09	0.07
CVRMSE	1.28	1.19	0.67	0.67

NRMSE, normalized root mean squared error; CVRMSE, covariance of root mean squared error.

Statistical downscaling of temperature and precipitation

Calibration and validation of SDSM. The explained variance E, coefficient of determination R^2 and Standard Error (SE) for maximum and minimum air temperature, and daily precipitation at the four sub-basins in the study area given in Table VI show that the model is capable of explaining more than about 66% and 60% of the variance in maximum and minimum air temperature, respectively, whereas only about 20% of the variance in daily precipitation can be explained by it. The plot in Figure 5 shows that there is good agreement between the observed and NCEP simulated maximum and minimum temperatures throughout the year during the validation period.

The low explained variance and R^2 obtained for daily precipitation exposes the difficulty of downscaling local precipitation series from regional scale predictor variables. Table VII compares the statistical regression model estimates of daily precipitation for the validation period with the observed series in terms of the bias, that is, the difference between the NCEP downscaled value and the observed value of the statistic. It is evident that the downscaling model produces lower estimates of percent of wet days and dry-spell length compared with those recorded in the study area. However, the downscaling

Table VI. Explained variance (E), R^2, and SE for precipitation, and maximum and minimum temperatures during the calibration period (1969–1979)

Sub-basin	Precipitation			Max. temperature			Min. temperature		
	E (%)	R^2	SE (mm)	E (%)	R^2	SE (mm)	E (%)	R^2	SE (mm)
1	18.5	0.26	0.3	68.1	0.83	0.39	60.6	0.82	0.35
2	20.6	0.18	0.37	70.4	0.87	0.42	64	0.84	0.35
3	21.1	0.25	0.31	70.4	0.87	0.42	64	0.84	0.35
4	21.3	0.30	0.3	66.9	0.82	0.4	57.2	0.81	0.32

model yielded higher estimates of daily mean precipitation compared with the observed values. As the E statistic or bias alone cannot evaluate the performance of the precipitation regression model, during the calibration and validation of precipitation downscaling models, the average daily precipitation, average monthly precipitation, average monthly percent of wet days, average monthly dry-spell lengths, and monthly variance in precipitation can be also used as performance criteria.

The results of precipitation downscaling using SDSM are found to be poor. Hence, the support vector machine (SVM) approach is adopted to downscale the mean areal precipitation of the sub-basins. SVM has proved to be a popular method to downscale precipitation, and the details can be found in Tripathi *et al.* (2006), Anandhi *et al.* (2008), Ghosh (2010), and Raje and Mujumdar (2011). The least square SVM (LS-SVM) has been used in the present study with a radial basis function (RBF) as kernel. The linear correlation coefficient or R-value obtained is used as an index to assess the performance of the LS-SVM with RBF kernel model and for fixing the parameters, RBF kernel width (σ), and the penalty parameter (C). The final values used in the model are $\sigma = 500$ and $C = 100$. In SVM downscaling method, the first 12 principal components of the NCEP climate variables (surface-specific humidity, mean sea level pressure, surface air temperature, precipitation flux, surface U-wind and surface V-wind, relative humidity, geopotential height) are directly used in fitting the

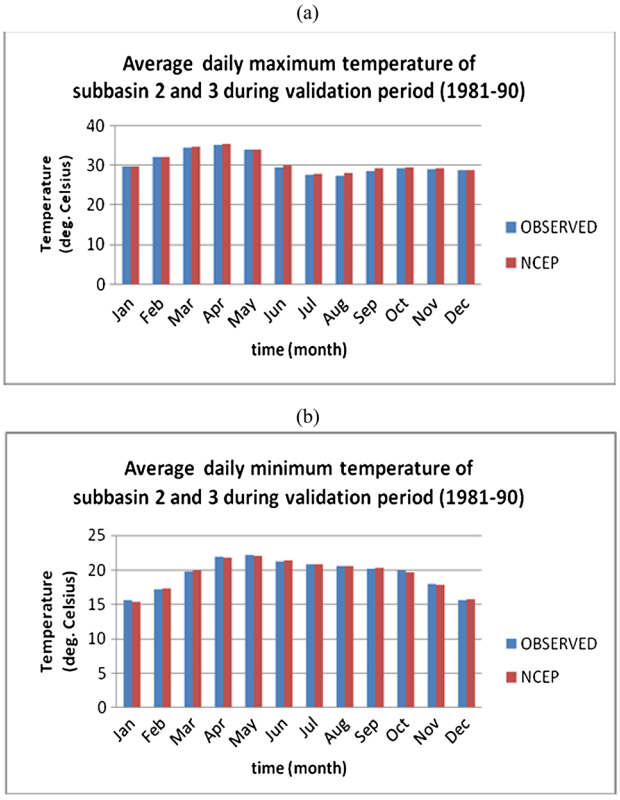

Figure 5. Comparison plots of observed and NCEP simulated (using SDSM) average daily (a) maximum and (b) minimum temperatures in sub-basins 2 and 3 during the validation period (1981–1990)

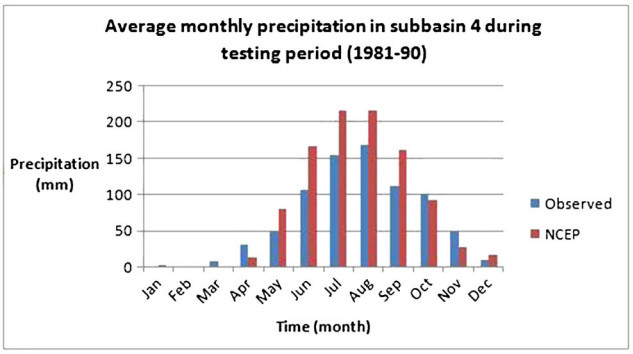

Figure 6. Comparison plots of observed and NCEP simulated (using SVM) average monthly precipitation during the testing period (1981–1990)

Table VII. Bias between the statistics of observed and NCEP simulated precipitation values during validation period (1981–1990)

Sub-basin	Mean (mm/day)			Variance (mm^2)			Percent of wet days			Dry-spell length (days)		
	Obs.	NCEP	Bias	Obs.	NCEP	Bias	Obs.	NCEP	Bias	Obs.	NCEP	Bias
1	3.53	4.95	1.42	26.91	19.37	−7.54	60.37	40.65	−19.7	5	5	0
2	4.06	4.12	0.07	44.54	38.77	−5.77	45.94	39.28	−6.7	6	5	−1
3	2.66	2.91	0.24	19.05	15.74	−3.32	60.29	44.68	−15.6	6	4	−2
4	4.17	4.46	0.29	34.67	28.60	−6.07	56.19	41.28	−14.9	6	5	−1

regression equation. In this study, NCEP data and observed monthly mean areal precipitation data of sub-basin 4 for a period of 1961 to 1980 are used to calibrate the model, and the data for the period of 1981 to 1990 are used for validation.

During training (calibration) and testing (validation) periods, the coefficient of determination is obtained as 0.99 and 0.81, respectively, with this data-driven technique. The SVM method thus showed improved performance compared with the SDSM. Figure 6 shows the comparison of observed and NCEP simulated monthly mean areal precipitation in sub-basin 4 obtained during testing of the SVM.

Projections of temperature based on downscaling. The increase in maximum and minimum daily temperature in the future periods under the two scenarios in all sub-basins is shown in Table VIII. The maximum daily temperature in sub-basins 2 and 3 under A2 scenario increased the most, i.e. by 1, 2.1, and 3.4 °C respectively, in the 2020s, 2050s, and 2080s.

Plots showing the projected diurnal variations in temperature in the four sub-basins of the study area for the future periods under the A2 and B2 scenarios are shown in Figures 7 and 8, respectively. The diurnal range decreased in the winter months and increased in months of July and August in sub-basins 1 and 4 under both scenarios, whereas in sub-basin 2, there is a considerable increase in diurnal range throughout the year.

Table VIII. Projected changes in maximum and minimum daily temperatures in the study area

Sub-basin	Change in maximum temperature (°C)						Change in minimum temperature (°C)					
	2020s		2050s		2080s		2020s		2050s		2080s	
	A2	B2	A2	B2	A2	B2	A2	B2	A2	B2	A2	B2
1	0.1	0.1	0.3	0.2	0.4	0.3	0.2	0.2	0.4	0.3	0.5	0.4
2	1.0	1.1	2.1	1.7	3.4	2.5	0.1	0.2	0.3	0.3	0.4	0.4
3	1.0	1.1	2.1	1.7	3.4	2.5	0.1	0.2	0.2	0.3	0.3	0.4
4	0.2	0.2	0.4	0.3	0.6	0.4	0.1	0.2	0.2	0.3	0.3	0.3

Projections of daily mean areal precipitation based on downscaling. Figures 9 and 10 show the projections of average monthly precipitation in the four sub-basins in the study area by SDSM, for the baseline and future periods under the A2 and B2 scenarios, respectively. The precipitation in the JJAS period in all sub-basins increased more under the A2 scenario than under B2. In the 2080s, in sub-basin 2, 75% and 58% increase in JJAS precipitation are projected under the A2 and B2 scenarios, respectively. The percent increase

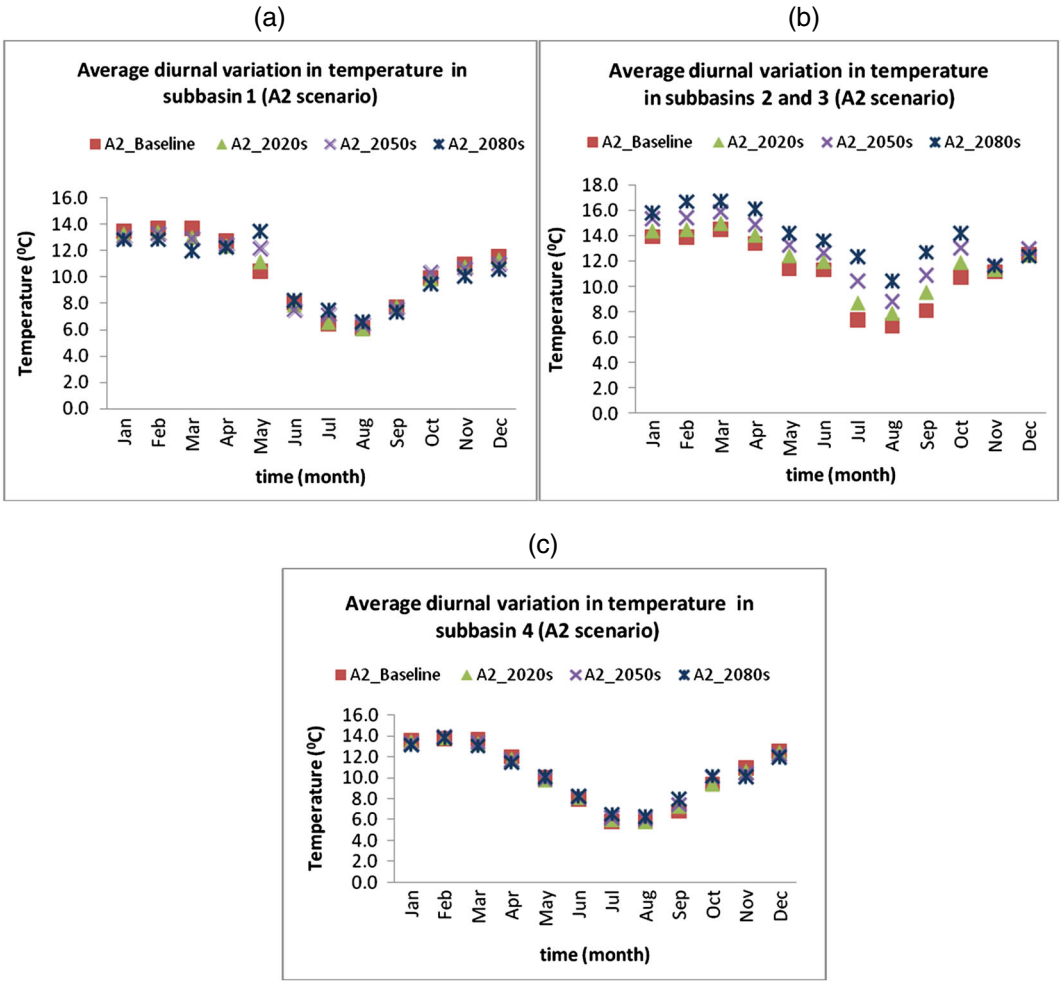

Figure 7. Plot showing observed and projected average diurnal variations in temperature in the four sub-basins of the study area under the A2 scenario

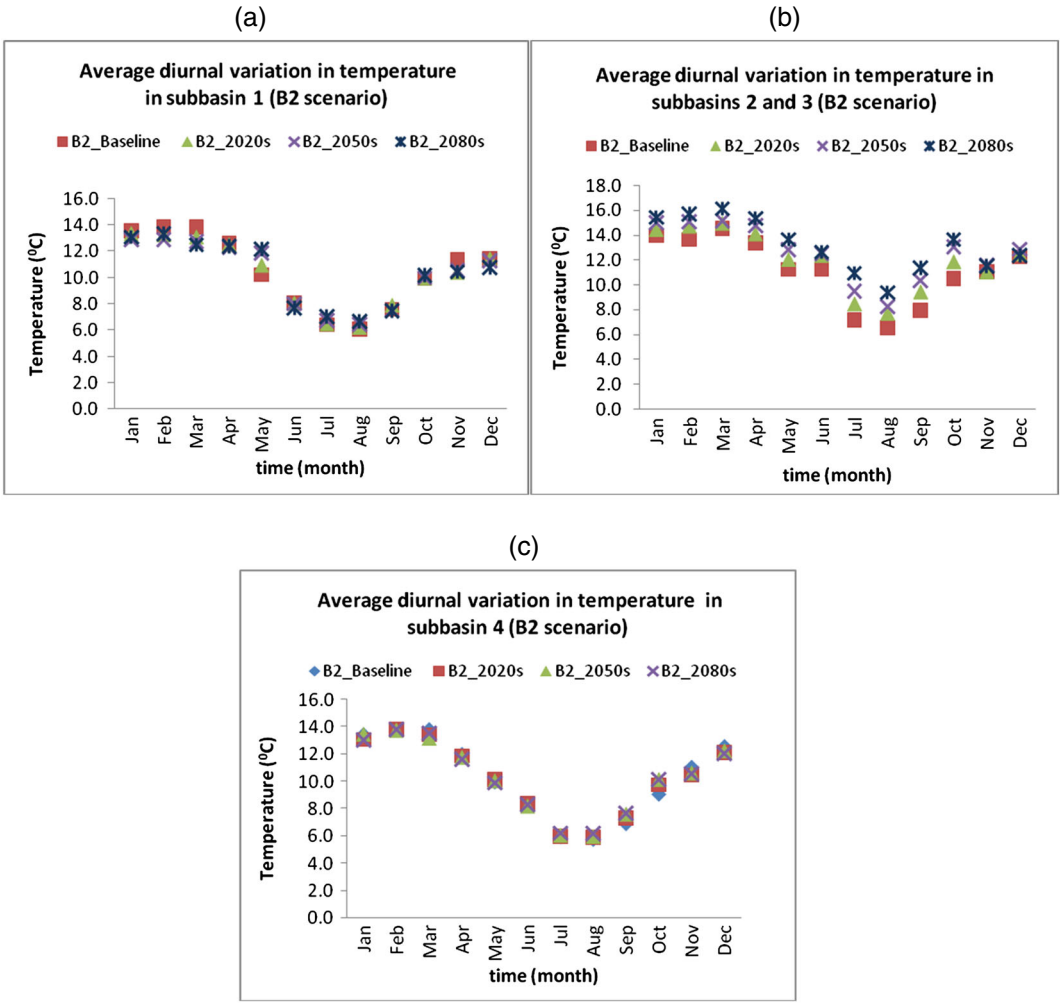

Figure 8. Plot showing observed and projected average diurnal variations in temperature in the four sub-basins of the study area under the B2 scenario

in sub-basin 4 is projected to be 15% in the 2020s, 28% in the 2050s, and 35% in the 2080s under the A2 scenario.

When the future projections for precipitation obtained from SVM downscaling are examined, increasing trends are observed with the A2 scenario. There is a marked increase in average monthly precipitation in most of the months with SVM as can be seen from the plots for sub-basin 4 under the A2 scenario in Figure 11. The difference between the projected monthly precipitation modelled by SDSM and SVM is very small. However, the future projections of monthly precipitation predicted is more with SDSM downscaling (Figure 9(d)) compared with SVM (Figure 11). For comparing the future projections obtained from the two downscaling methods, a plot of changes projected in the average monthly precipitation of sub-basin 4 under the A2 scenario is given in Figure 12. It is seen that for the months April, June, September, and November, both methods project an increase in precipitation, of varying amounts.

Validation of hydrological model with downscaled climate data

Flows are generated by giving both observed and downscaled (for the A2 and B2 scenarios of HadCM3) precipitation and temperature data for the current period 1973–1990 as inputs to the HEC-HMS 3.4 model of the study area. Likewise, the PET values are also simulated. Some statistical properties of the simulated streamflows during the period 1973–1990 corresponding to both observed and downscaled precipitation and temperature inputs given in Table IX show that the hydrological model with downscaled inputs mostly overestimates the mean streamflows in the basin whereas the model with observed inputs slightly underestimated the mean flows. However, they reproduced the variability better than observed data-driven model. The statistics of PET simulated in one of the sub-basins by using the observed inputs and the HadCM3 inputs for the period 1973–1990 is given in Table X. The mean, median, and standard deviation values are all simulated very well. It can be concluded on the basis of the above observations that the hydrological model used in the study effectively demonstrates the effect of the climate pattern found in the downscaled data.

Impacts of climate change on the hydrology of the basin

Changes in streamflows. It is seen that the A2 and B2 scenarios may produce a wide range of changes in the hydrology of the basin. It is clear from the box plots of predicted daily streamflows in Figure 13 for the three periods that streamflows are increasing in the future for

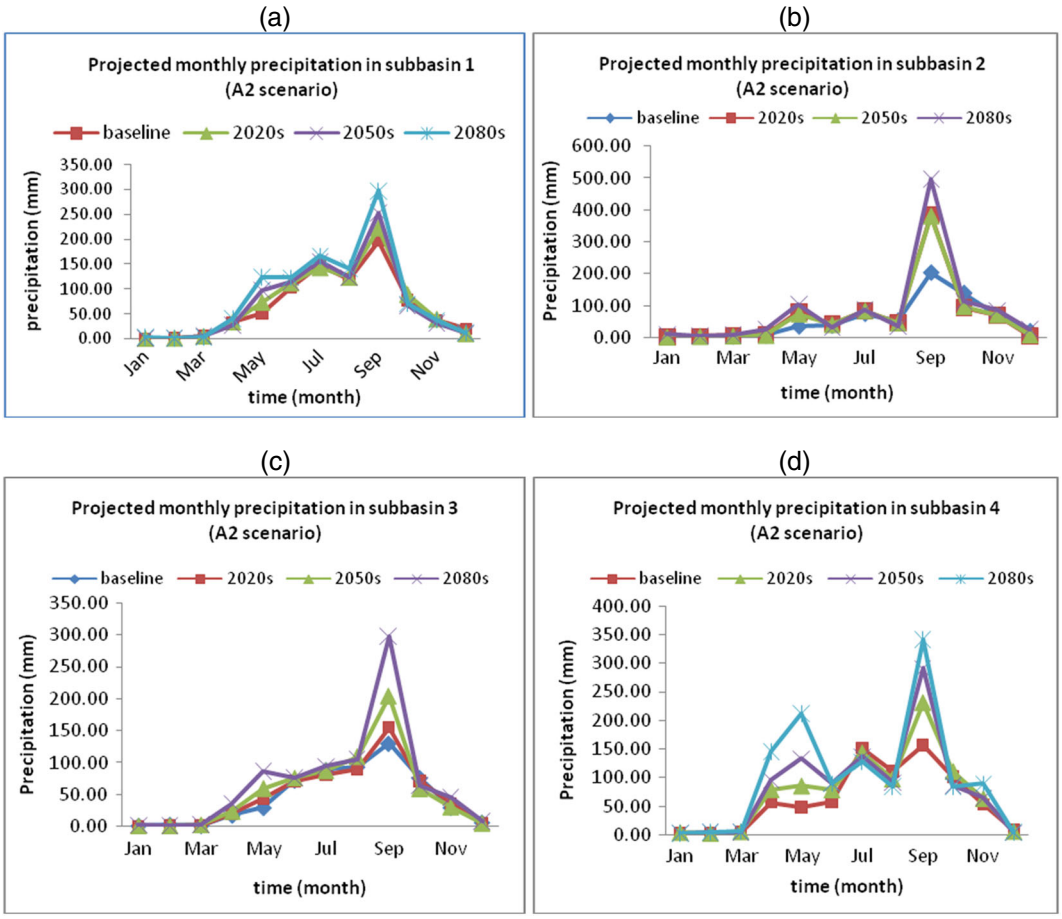

Figure 9. (a–d) Projections of average monthly precipitation in four sub-basins of the study area for the current and future periods under the A2 scenario

both scenarios. All periods under the A2 scenario showed an increase, of about 6.8 cumecs in the 2020s, 31.8 cumecs in the 2050s, and 74.2 cumecs in the 2080s in the mean flows. The mean flows in the baseline period of the B2 scenario was 124 cumecs, which is projected to 145.7 cumecs in the 2050s and 169 cumecs in the 2080s. Table XI shows the projected percent change in the average monthly streamflows in future periods under the A2 and B2 scenarios with respect to the baseline flows. The projected streamflows show a decline in the months December to March in all the three future periods under the A2 and B2 scenarios. There is an increasing tendency in the flows of April in the 2080s under the A2 scenario. Streamflows in May, June, July, and September also showed increasing trend in all three periods under both scenarios, although in August the trend is a decrease. The magnitude of increase projected is higher in the A2 scenario compared with B2 scenario. The average annual streamflows project an increase of 4%, 17.1%, and 43.9%, respectively, in the 2020s, 2050s, and 2080s under the A2 scenario and an increase of 5.4% and 18.5%, respectively, in the 2050s and 2080s under the B2 scenario, with respect to the baseline flows. The average monthly streamflows simulated under the A2 and B2 scenarios for the baseline and the three future periods are shown in Figure 14(a and b). The flows in the months of May, June, July, and September are projected to increase under the A2 and B2 scenarios. The flows in the months of August and October projected to decrease under both scenarios. The changes predicted in the flows during summer (March, April) and winter (November–February) months are negligible, as already the flows are very low during these periods.

Changes in potential evapotranspiration. It is observed from the box plots of projected daily PET values under the A2 scenario in Figure 15 that in sub-basins 1 and 4, the average daily PET slightly reduced compared with the baseline value, whereas in sub-basins 2 and 3, there is a gradual increase in the average values in the future period under the A2 scenario. Similar trends are observed in the projected PET values under the B2 scenario from the box plots in Figure 16.

The projected changes (in percentage) are shown in the plots in Figure 17. The average daily PET value projected in sub-basin 1 decreases by 3.7% in the 2020s, 3% in the 2050s, and 3.6% in the 2080s under the A2 scenario. The average daily PET value projected in sub-basin 2 under the B2 scenario increases by 18% in the 2020s, 22% in the 2050s, and 29% in the 2080s. The average daily PET value projected in sub-basin 2 under the A2 scenario increases by 1.5% in the 2020s and 2050s and 16.7% in the 2080s. The average monthly PET values in sub-basins 2 and 3 are also projected to increase in the future periods under the A2 and B2 scenarios.

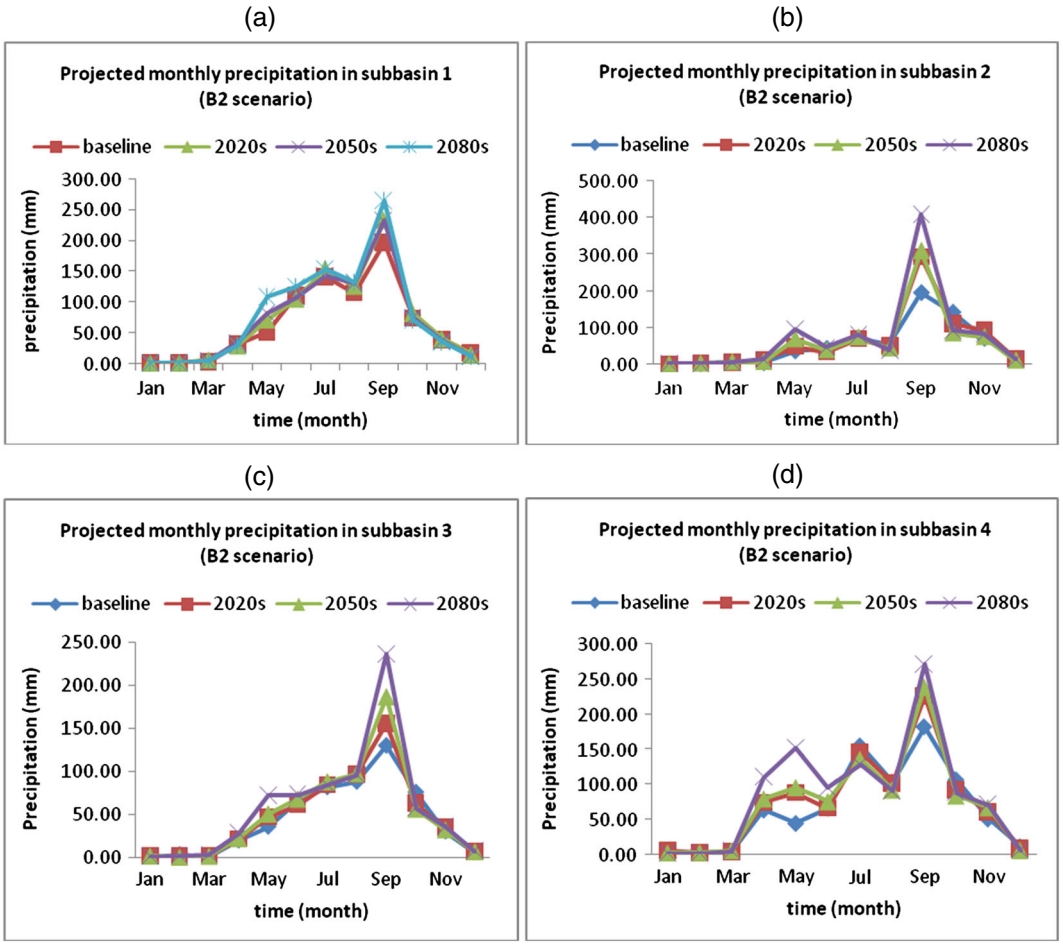

Figure 10. (a–d) Projections of average monthly precipitation in four sub-basins of the study area for the current and future periods under the B2 scenario

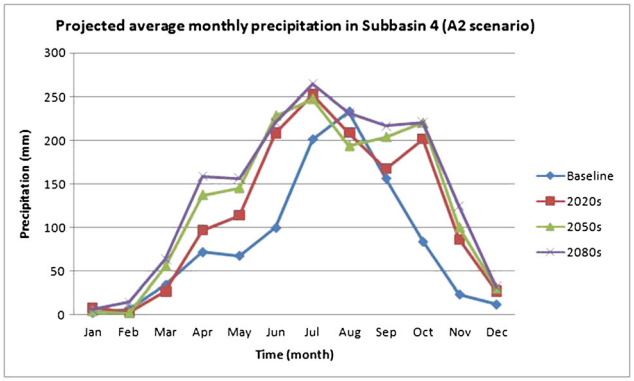

Figure 11. Projections of average monthly precipitation in sub-basin 4 for the current and future periods under the A2 scenario by SVM

Changes in water balance. The projected percentage change in annual actual evapotranspiration (AET) losses in the future periods under both scenarios is listed in Table XII. Under the A2 climate scenario, the AET losses in the study area are projected to increase in sub-basins 1, 2, and 3, in the 2050s and 2080s. However, under the B2 scenario, in sub-basin 3, the AET values are projected to decrease. In sub-basin 4, under both scenarios, AET losses are predicted to decrease in the future periods. The future trend in the contribution of annual precipitation to various water balance components in the basin such as excess rainfall, AET, and percolation (infiltration) are shown in the plots of Figure 18. The contribution of precipitation to AET loss is projected to decrease in all sub-basins under the A2 as well as B2 scenario. In sub-basins 1 and 3, the contribution to infiltration losses is expected to increase under both scenarios, whereas in sub-basins 2 and 4, this component is negligible. Whereas the percentage of rain contributing to direct runoff decreases in sub-basin 1 under both scenarios, in sub-basin 3, a small increase is projected. In sub-basins 2 and 4, there may be increase in the surface runoff component. The average annual water balance of each of the four sub-basins has been projected to change in different ways, so an attempt to generalize the nature of change in water balance of the region is performed. The likely changes in water balance components aggregated for the study area under the two scenarios compared with the baseline period is also computed and listed in Table XIII. About 28% increase in future precipitation simulated by the HadCM3 A2 scenario in the 2080s projected to produce 46% increase in surface runoff, a 5% decrease in AET, and an 88% increase in percolation, in the study area on an annual basis. Similarly, a 50% increase in future precipitation simulated by the HadCM3 B2 scenario in the 2080s predicted to lead to 103% increase in surface runoff, a 6% decrease in actual evapotranspiration, and a 117% increase in percolation.

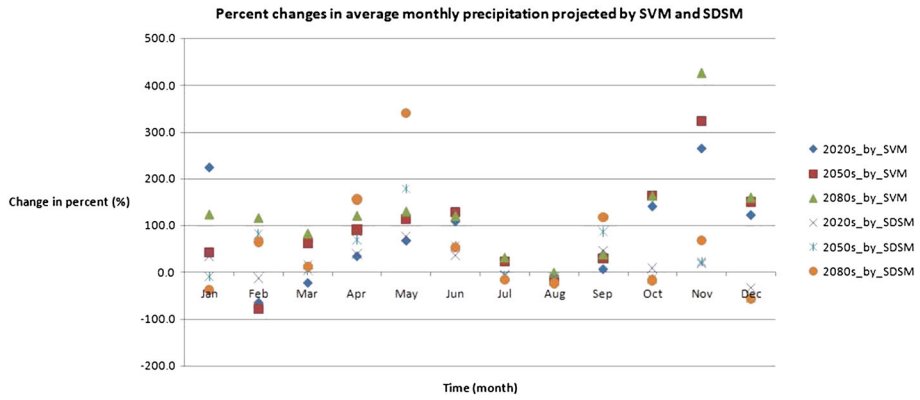

Figure 12. Comparison of percent change in average monthly precipitation of sub-basin 4 projected by SVM and SDSM

Table IX. Statistics of the observed and simulated (with HadCM3 downscaled A2, B2, and observed inputs) discharges at the outlet of the basin

Statistic (cumecs)	Baseline_A2	Baseline_B2	Historic observed	Observed
Mean	273.0	279.4	219.8	225.3
SD	379.9	383.2	343.2	386.5
Minimum	24.9	25.0	24.8	2.4
Maximum	3575.0	2930.4	7402.2	4562.0

SD, standard deviation.

Table X. Statistics of the simulated (with HadCM3 downscaled A2, B2, and observed inputs) potential evapotranspiration (PET) in sub-basin 1

Statistic (mm)	Observed	Baseline_A2	Baseline_B2
Mean	5.2	5.16	5.18
Median	4.87	4.88	4.89
SD	0.97	0.94	0.95

SD, standard deviation.

CONCLUSIONS

The present case study aimed to create a hydrological model of the catchment area of River Tunga-Bhadra, lying upstream of the Tungabhadra dam, and assess the impacts of climate change on the hydrology of the basin.

Table XI. Projected percent change in monthly streamflows at the outlet of the basin under different scenarios

	A2			B2		
Month	2020s	2050s	2080s	2020s	2050s	2080s
Jan	−32.3	−34.0	−31.0	−31.8	−33.4	−34.4
Feb	−55.0	−55.2	−55.0	−56.3	−56.1	−55.2
Mar	−56.6	−56.2	−55.3	−56.3	−55.8	−54.8
Apr	−19.9	−20.4	87.9	−26.2	−12.2	−8.3
May	36.0	164.4	776.2	15.7	78.4	272.6
Jun	45.3	208.7	358.0	32.5	104.4	339.9
Jul	12.2	28.7	30.4	11.9	21.2	27.4
Aug	−18.3	−20.1	−22.3	−16.7	−19.0	−18.8
Sep	29.5	59.6	94.5	15.2	22.2	45.3
Oct	−1.0	−10.3	−1.8	−14.0	−13.1	−20.6
Nov	−4.6	−15.0	−2.7	−0.7	3.6	−11.6
Dec	−27.7	−33.7	−10.2	−22.3	−21.3	−21.4
Annual	4.0	17.1	43.9	−1.3	5.4	18.5

The hydrology of the basin is modelled quite well by the HEC-HMS 3.4 hydrological model except for the high flows. Under-prediction of high flows is an inherent problem seen in hydrological modelling of the basin in the case study. This is due to the lack of extreme event modelling capability of the hydrological model. The monthly flows are better simulated than daily flows.

The climate variables obtained as output from a coarser resolution GCM, HadCM3 model is then downscaled to obtain finer resolution inputs required by the hydrological

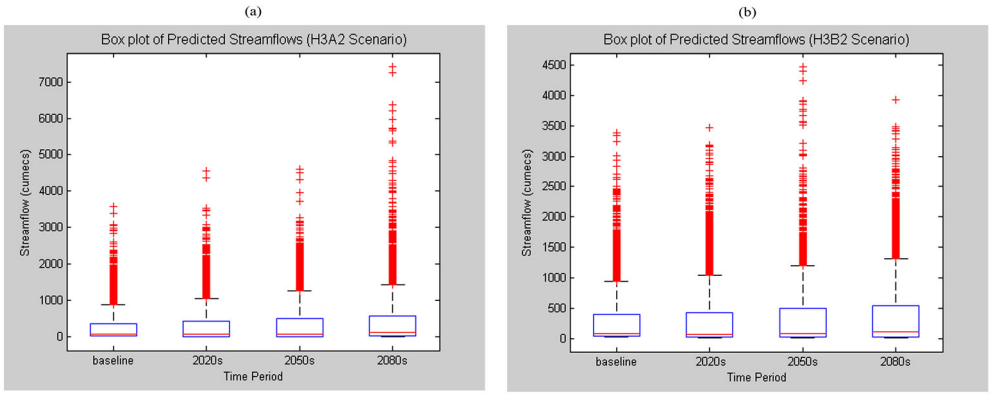

Figure 13. Box plots of baseline and future daily streamflows simulated under the (a) A2 and (b) B2 scenarios

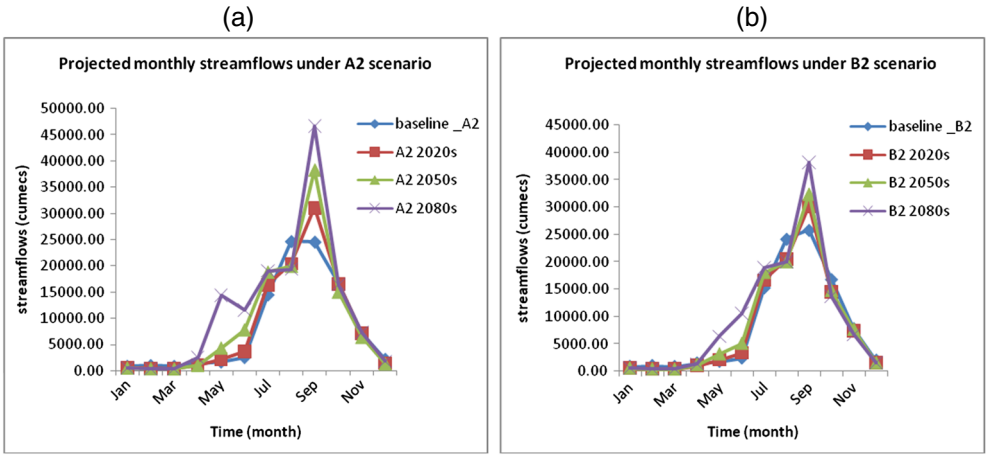

Figure 14. Comparison between the baseline and projected average monthly flows in the various time periods under the (a) A2 and (b) B2 scenarios

model using SDSM 4.2. The statistical downscaling procedure performed well for the maximum and minimum temperature but poorly for the daily mean areal precipitation. The low explained variance and R^2 value for daily precipitation highlighted the difficulty of downscaling local daily precipitation series from regional scale predictor variables. The inherent statistical properties of the precipitation data make it difficult to set up a good downscaling model. The temperature projections for the future indicate an increase in the maximum and minimum daily temperature compared with the baseline period. There is a larger increase in maximum temperature under the A2 scenario than B2. The daily precipitation values of summer months are projected to increase in sub-basin 4 in the future under both scenarios. The winter months except January are however projected to change less in terms of daily precipitation. The precipitation in the JJAS period in all sub-basins increased more under the A2 scenario than under the B2 scenario. The increase amounted to about 50% in the 2050s and 75% in the 2080s under the A2 scenario in sub-basin 2. Another method, SVM, is used to downscale the precipitation values to examine the performance and to compare with the present results. SVM performed well compared with SDSM in terms of R^2 value. However, the hydrological model HEC-HMS is run for the future with SDSM downscaled outputs despite its poor performance as

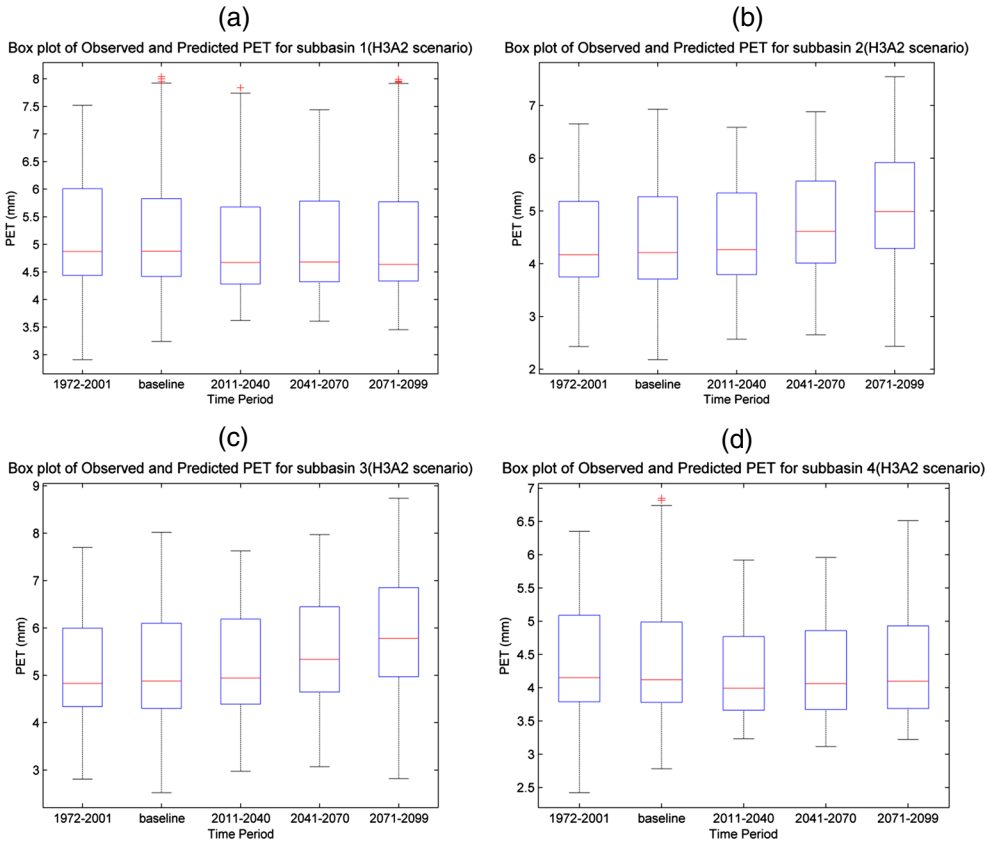

Figure 15. Box plots showing projected daily PET values in the four sub-basins in the baseline and future periods under the A2 scenario

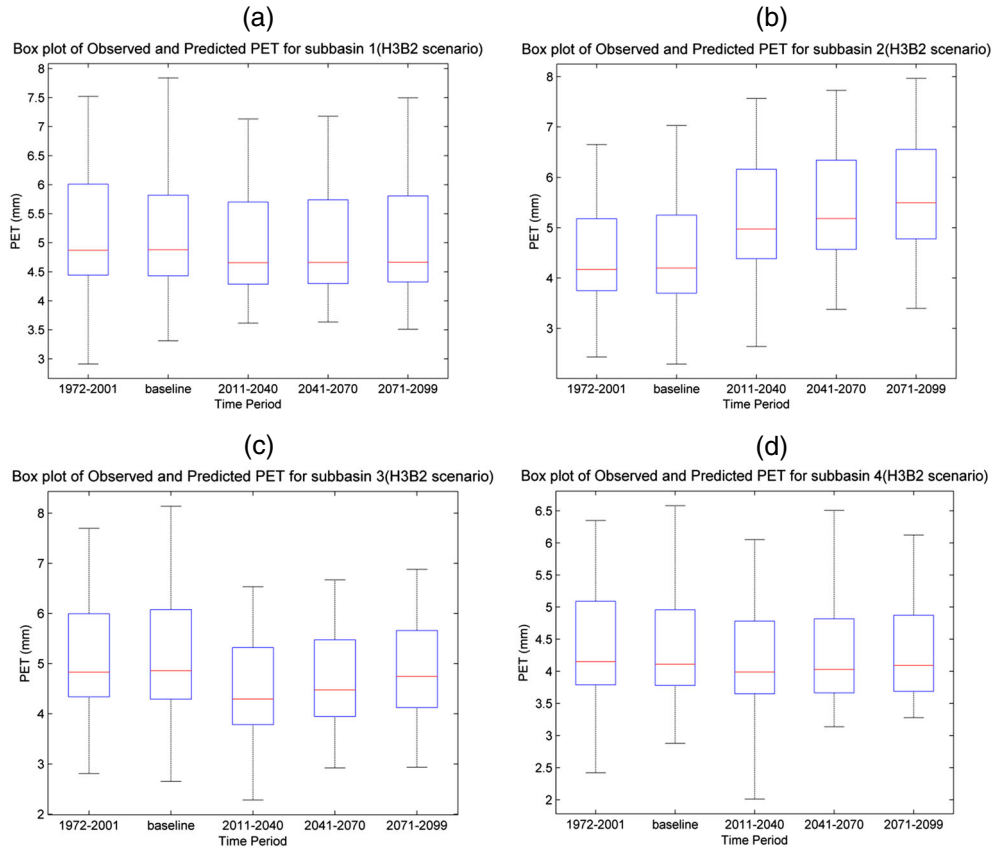

Figure 16. Box plots showing projected daily PET values in the four sub-basins in the baseline and future periods under the B2 scenario

the results of SDSM do not deviate much from SVM downscaling results.

The performance of the hydrological model in climate change impacts assessment is looked into by comparing the baseline flows under both scenarios, with the observed flows. The validated model when provided with the future climate variables, i.e. temperature and daily rainfall values as inputs, generated the future streamflows at the outlet of the basin. The impacts of climate change on the hydrology of the study area are then investigated by comparing the flows, PET, and water balance during the baseline (1961–90) and the future periods (2020s, 2050s, and 2080s).

Streamflows in May, June, July, and September increased in all three periods in both scenarios, although in August, a decreasing trend is observed. The magnitude of increase in flows is observed to be more under the A2 scenario than B2. The average annual streamflows record an increase of 4%, 17.1%, and 43.9%, respectively, in the 2020s, 2050s, and 2080s under the A2 scenario and an increase of 5.4% and 18.5%, respectively, in the 2050s and 2080s under the B2 scenario. The projected PET values in sub-basins 1 and 4 show a slight reduction compared with the baseline values. The average monthly PET values in sub-basins 2 and 3 are projected to increase in the future periods under the A2 and B2 scenarios. The average daily PET value projected in sub-basin 2 under the A2 scenario increases by 1.5% in the 2020s and 2050s and 16.7% in the 2080s. The increase observed is more

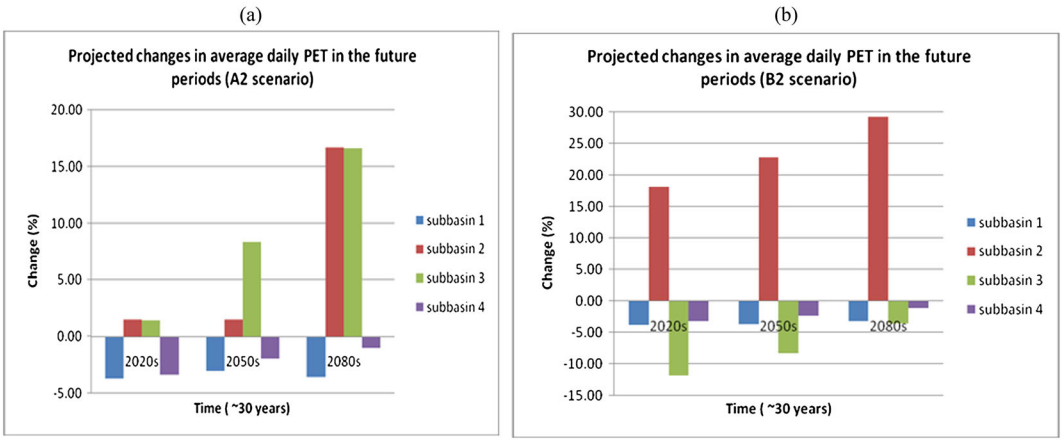

Figure 17. Projected changes in the average daily PET values in the future periods under the (a) A2 and (b) B2 scenarios in the four sub-basins

Table XII. Projected percent change in AET component from baseline to future scenarios in the four sub-basins

Sub-basin	2020s		2050s		2080s	
	A2	B2	A2	B2	A2	B2
1	8.3	10.5	7.9	3.1	4.6	7.2
2	8.7	7.6	10.1	8.6	17.9	24.7
3	−2.2	−5.7	0.5	−5.5	1.7	−2.4
4	0.4	−2.7	−1.5	−8.9	−5.2	−12

Table XIII. Projected percent change in overall water balance components of the study area from baseline to future scenarios

Component	A2			B2		
	2020s	2050s	2080s	2020s	2050s	2080s
Precipitation	12.4	14.8	27.7	15.0	23.9	50.6
Excess rainfall	18.8	26.6	46.3	37.1	52.9	103.9
AET	−5.5	−5.2	−4.7	−7.5	−10.4	−5.9
Percolation	53.7	50.9	87.6	40.4	71.2	117.4

under the B2 scenario in the two sub-basins 2 and 3. Water balance studies of all sub-basins are carried out for the future periods under the A2 and B2 scenarios. The trends projected for various components differ from sub-basin to sub-basin. Therefore, the results of four sub-basins are aggregated to represent the water balance of the study area as a whole. A 28% increase in future precipitation simulated by the HadCM3 A2 scenario in the 2080s produced a 46% increase in direct runoff, a 5% decrease in AET, and a 88% increase in infiltration, in the study area on an annual basis. Similarly, 50% increase in future precipitation simulated by the HadCM3 B2 scenario in the 2080s produced a 103% increase in direct runoff, a 6% decrease in AET, and a 117% increase in infiltration.

The possible changes projected by the study provide a useful input to effective planning of water resources of the study area. The study is intended to cater to the research on climate impact studies in developing countries, using freely available and less data-intensive models. In short, the study aimed at creating awareness, as to how the possible climate change can affect the water resources at local level and the need for modifying the existing water infrastructure in the region to sustain the water resources systems against future climate change.

LIMITATIONS OF THE STUDY

The study of impacts of climate change on the hydrology of catchment area of the Tunga–Bhadra River lying upstream of the Tungabhadra dam is carried out by coupling a single hydrological model and downscaling results obtained from a single GCM. The hydrological

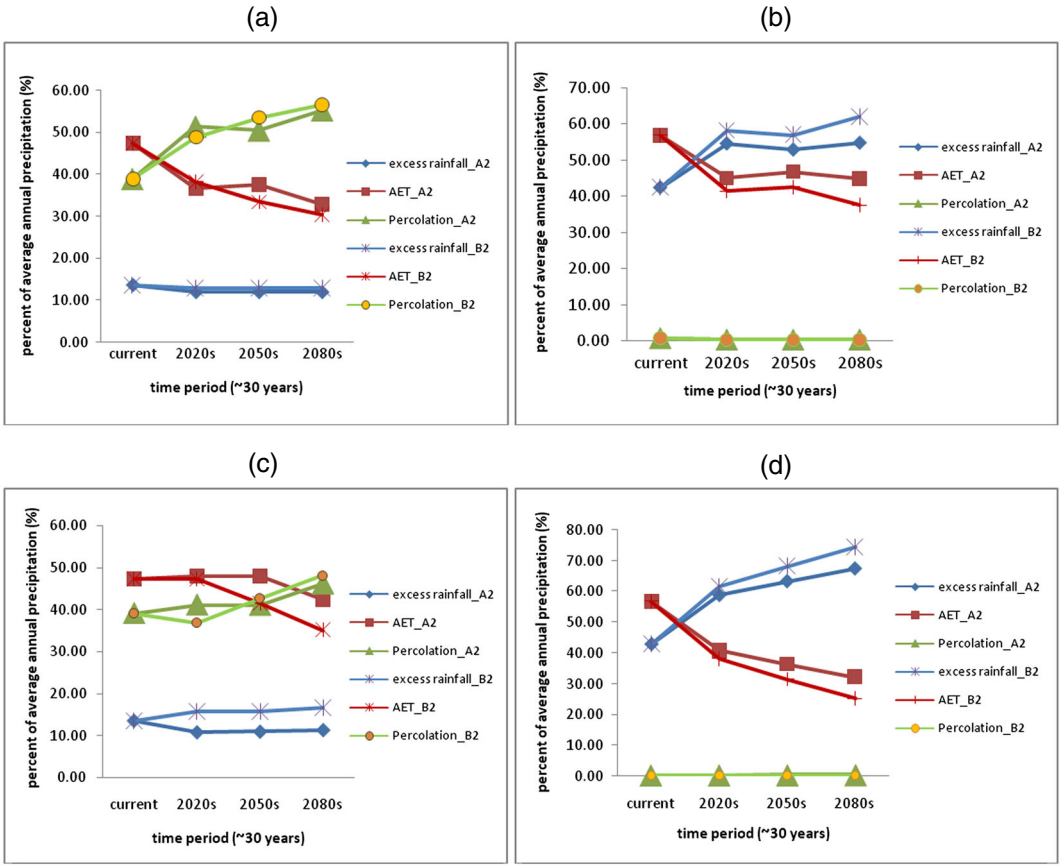

Figure 18. Plots showing projected percentage of contribution of annual precipitation to the water balance components in the four sub-basins of the study area under the A2 and B2 scenarios

model underpredicted the high flows (flows during JJAS period). Efforts were made to address the uncertainty involved in the results of the present model by looking into the magnitude of underprediction. Therefore, the future scope of the work should be to develop a hydrologic model that can accommodate extreme event modelling capabilities. However, limitations also arise because of several assumptions involved in the various steps of modelling. Similarly, the performance of SDSM 4.2 is not found appreciably good in downscaling daily precipitation. So, a precipitation downscaling study is carried out using the SVM technique and is found to perform very well.

The land use pattern is assumed to be the same in this study. If a changed pattern of the same is assumed, the results would have been different. Thus, the use of different models and methodologies in hydrological modelling and downscaling may lead to different results and different conclusions. Hence, there are several uncertainties to be addressed, by comparing the results of varied methodologies adopted for the same site and period.

REFERENCES

Anandhi A, Srinivas VV, Nanjundiah RS, Kumar DN. 2008. Downscaling precipitation to river basin in India for IPCC SRES scenarios using support vector machine. *International Journal of Climatology* **28**: 401–420.

Christensen NS, Wood AW, Voisin N, Lettenmaier DP, Palmer RN. 2004. The effects of climate change on the hydrology and water resources of the Colorado River basin. *Climatic Change* **62**: 337–363.

Chu JT, Xia J, Xu CY, Singh VP. 2010. Statistical downscaling of daily mean temperature, pan evaporation and precipitation for climate change scenarios in Haihe River, China. *Theoretical and Applied Climatology* **99**: 149–161.

Dibike YB, Coulibaly P. 2005. Hydrologic impact of climate change in the Saguenay watershed: comparison of downscaling methods and hydrologic models. *Journal of Hydrology* **307**(1–4): 145–163.

Dibike YB, Coulibaly P. 2007. Validation of hydrological models for climate scenario simulation: the case of Saguenay Watershed in Quebec. *Hydrological Processes* **21**(23): 3123–3135.

Ghosh S. 2010. SVM-PGSL coupled approach for statistical downscaling to predict rainfall from GCM output. *Journal of Geophysical Research* **115**: D22102. DOI: 10.1029/2009JD013548

Google Earth 2010. 2009. River Tunga–Bhadra.

HWSD Viewer 1.1. 2009. Harmonized World Soil Database (HWSD), version 1.1.

Jha M, Arnold JG, Gassman PW, Giorgi F, Gu RR. 2006. Climate change sensitivity assessment on Upper Mississippi River Basin streamflows using SWAT. *Journal of the American Water Resources Association* **42**(4): 997–1015.

Jiang T, Chen, YD, Xu C-Y, Chen XH, Chen X, Singh VP. 2007. Comparison of hydrological impacts of climate change simulated by six hydrological models in the Dongjiang Basin, South China. *Journal of Hydrology* **336**: 316–333.

Nash JE, Sutcliffe JV. 1970. River flow forecasting through conceptual models part 1—a discussion of principles. *Journal of Hydrology* **10**(3): 282–290.

Raje D, Mujumdar PP. 2011. A comparison of three methods for downscaling daily precipitation in the Punjab region. *Hydrological Processes*. DOI: 10.1002/hyp.8083

Rehana S, Mujumdar PP. 2011. River water quality response under hypothetical climate change scenarios in Tunga–Bhadra river, India. *Hydrological Processes*. DOI: 10.1002/hyp.8057

Singh VP, Woolhiser DA. 2002. Mathematical modeling of watershed hydrology. *Journal of Hydrologic Engineering* **7**(4): 270–292.

Sorooshian S, Gupta VK. 1995. Model calibration. Chapter 2 In *Computer Models of Watershed Hydrology*, Singh VP (ed). Water Resources Publications: Littleton, CO; 23–68.

STRIVER. 2009. Task Summary Report No. 9.3. Land use and land use change—implications for water resources and water use in the Tagus and Tungabhadra Basins.

Tripathi S, Srinivas VV, Nanjundiah RS. 2006. Downscaling of precipitation for climate change scenarios: a support vector machine approach. *Journal of Hydrology* **330**(3–4): 621–640.

US Army Corps of Engineers. 2008. HEC HMS User Manual version 3.2. Davis, CA.

Wilby RL, Hay LE, Leavesley GH. 1999. A comparison of downscaled and raw GCM output: implications for climate change scenarios in the San Juan River basin, Colorado. *Journal of Hydrology* **225**: 67–91.

Xu ZX, Zhao FF, Li JY. 2009. Response of streamflow to climate change in the headwater catchment of the Yellow River basin. *Quaternary International* **208**: 62–75.

Yimer G, Andreja J, Griensven AV. 2009. Hydrological response of a catchment to climate change in the Upper Beles River basin, Upper Blue Nile, Ethiopia. *Nile Basin Water Engineering Scientific Magazine* Vol. 2.

Yu PS, Wang YC. 2009. Impact of climate change on hydrological processes over a basin scale in Northern Taiwan. *Hydrological Processes* **23**: 3556–3568.